

HIGHLIGHTS OF PREPARATIVE SOLID STATE CHEMISTRY IN LOW PRESSURE PLASMAS

Stanislav Vepřek

Institute of Inorganic Chemistry, University of Zürich,
Winterthurerstrasse 190, 8057 Zürich, Switzerland

Abstract - Most of the work in cold plasmas was devoted to the heterogeneous solid-gas system. A notable exception to this is ozone synthesis.

With regard to industrial applications, low pressure plasmas are being currently applied mainly to thin film deposition in the manufacturing of integrated microcircuits, optical fibres and protective coatings. Low deposition temperatures, sufficiently high deposition rates, excellent physical and chemical properties of the films and their good adherence to the substrate were recognized as the main advantages of plasma technology.

The preparation of hydrogenated, fluorinated and chlorinated amorphous and microcrystalline silicon is of large interest with respect to industrial applications as well as to basic research. Indeed, the successful demonstration of the substitutional doping of a-Si by Spear and Le Comber and, independently, by Carlson, et al. five years ago opened the way toward its applications in electronic devices (solar cells, rectifiers, and others) and attracted large attention to this material. The heterogeneous Si/H-plasma system is an excellent example of the variety and achievements of plasma chemistry and, therefore, it is discussed in some detail here.

The plasma assisted preparation of new materials or of known materials having new, unique properties, brings plasma chemistry close to the field of solid state chemistry and physics. Further progress can, no doubt, be achieved only by combining sufficient knowledge and experience from all the disciplines involved. Moreover, examples such as the synthesis of rare gas compounds and of complex compounds show that preparative plasma chemistry can also bring new aspects and innovative ideas to the true chemists who love the beauty of variety.

INTRODUCTION

A typical and serious drawback of the plasma-chemical processes in the gas phase is their poor selectivity resulting in unacceptably low reaction yields. This is due to competing processes which take place simultaneously with the formation of the desirable products, either in the discharge zone or in the afterglow. Typical examples of industrially important processes of this kind are the conversion of methane to acetylene in thermal plasmas (1) and the synthesis of ozone in a silent discharge (2,3). The problem is inherent to the plasma-chemical processes since the desirable gaseous products are endothermic compounds which are likely to be decomposed by fast radical and ion-molecule reactions, unless extremely sophisticated quenching procedures are applied. Thus, not only high quenching rates of $\geq 10^6$ K/sec, but also a carefully optimized flow geometry and the moment of the application of quenching to the gas are necessary in order to achieve an acceptable degree of conversion in the thermal plasmas. Similarly, a sophisticated, pulsed spatially homogeneous glow discharge is required for ozone synthesis in a "cold plasma" (2-4). As a result, the price of the final product is dominated by high capital costs making it difficult for the plasma-chemical processes, in spite of their other advantages, to compete with conventional ones.

The ozone synthesis is among the rare exceptions to this rule because there is no other method for its large scale industrial production. Ecological problems associated with the application of chlorine for the treatment of drinking-, cooling- and waste water make its replacement by ozonization necessary in the near future. For similar reasons, ozone will be used in many other industrial processes, such as bleaching and oxidation. The resulting future demands on its production call for a large research and development effort in order to improve the efficiency of its production, as well as the specific production rate density (expressed in terms of kg of O₃ produced per hour divided by the total volume of the production unit) (2-6).

The selectivity of the plasma-chemical processes is automatically improved in the heterogeneous systems solid/gas, particularly if the solid phase can be maintained in a quasi-equilibrium state with the plasma as is the case in non-isothermal, low pressure plasmas. The manifold possibilities in which the solid can dissipate the energy deposited in various forms (electronic, vibrational, kinetic, radiation) on its surface causes many of the chemical reactions taking place in the gas phase to become ineffective or modified at the surface. Consequently, the chemistry of such systems is dominated by the reactions of atoms and radicals and, in the case of a sufficient negative bias, by momentum transfer-induced processes due to ion-bombardment. Because of the non-isothermal nature of low pressure plasmas these reactions proceed with high rates at reasonably low temperatures which are required in various industrial processes, the fabrication of electronic devices being the most important and typical one. Since capital costs for the low pressure plasma generation, and the amount of the solid material to be processed are also relatively low, plasma etching and chemical vapour deposition are the most promising processes to meet the requirements for large-scale applications in various branches of industry.

In addition there are further, unique features of these processes which cannot be achieved by other conventional techniques. As an example let us mention the control of the isotropy during plasma etching which is required for fabrication of subminiaturized integrated circuits (7-10), and the deposition of dielectric and semiconducting films at low temperatures which, beside the electronic industry are receiving growing interest and applications in many further industrial branches. These aspects were reviewed in some recent (11-14) and earlier (7) papers and books.

In the present paper we shall restrict the discussion to few selected systems in order to provide a deeper insight into the processes determining the course of the chemical reactions taking place during deposition in the plasma and the properties of the deposit. Emphasis will be on the reversible chemical transformations, such as chemical transport, which provide the best control of the chemical evaporation and deposition under conditions of non-isothermal plasmas. The theoretical background illustrated by experimental results was given in earlier papers (15-18) and summarized in Ref. (11,19,20).

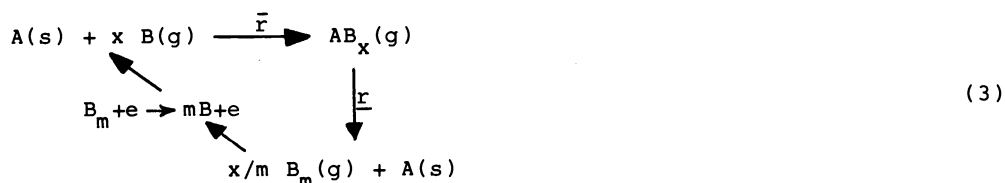
Briefly, the theoretical analysis and the experimental results show that, under certain conditions, reversible chemical equilibria can be established in non-isothermal plasmas corresponding to a thermodynamically non-equilibrium state with vanishing overall chemical fluxes. Examples of such equilibria were given (17,18) and the Si/H-system, to be discussed in this paper, represents the most illustrative example. During the deposition in the vicinity of such an equilibrium state, stable solid phases are typically obtained whereas metastable ones are being usually formed if the deposition takes place far away from chemical equilibrium, i.e. when reaction (1) takes place irreversibly from the right to the left hand side ($\bar{r} \gg \underline{r} \approx 0$):



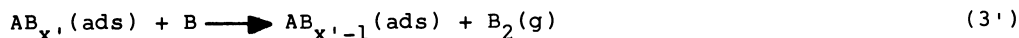
In the chemical equilibrium the rates of the forward and reverse reactions are equal, $\bar{r} = \underline{r}$, but the microscopic reversibility $a_i p_{ij} = a_j p_{ji}$ (a_i and p_{ij} are the occupation and transition probabilities related to the transitions between the i and j states) which applies to thermodynamic equilibrium is replaced by the more general balance criterion

$$\sum_j a_i p_{ij} = \sum_i a_j p_{ji} \quad (2)$$

Accordingly, a simplified scheme of reaction (1) under non-isothermal plasma conditions is given by eq. (3):



If, as in the majority of cases being studied so far, $AB_x(g)$ is thermodynamically unstable with respect to $A(s)$ and $B_m(g)$, the deposition takes place irreversibly in a weak discharge but it can be made reversible by increasing the degree of dissociation of B_m in the "charge zone" (see the electron impact induced dissociation in eq. (3)), e.g. due to an increase of the discharge current density. The forward reaction (\bar{r} - see eq. (3)) can take place only if it is exothermic and kinetically possible. The latter condition essentially requires that the rate of the competing processes which lead to the decomposition of $AB_x(ads)$ or of its precursors (e.g. $AB_{x-n}(ads)$) on the surface via different reaction channels is sufficiently slow to allow the formation of $AB_x(g)$. A typical example of such a competing process is the heterogeneous recombination, eq. (3'):



The rates of the forward reaction (\bar{r} , see eq. (3)) and of the recombination, eq. (3'), frequently display different temperature dependences which can be utilized to shift controllably the chemical equilibrium of reaction (1) and, thus, to perform the chemical transport of the solid $A(s)$.

CONTROL OF THE STRUCTURAL PROPERTIES OF THE DEPOSIT

The close relation between the structural perfection and the physical and chemical properties of the deposit brings us to the central problem of the control of the structure of the solid product during the deposition. A large part of the subsequent section on the preparation of silicon will be devoted to a discussion of the related problems. Here, we shall give a few selected examples to substantiate the general rules outlined above.

Amorphous carbon

Thin films of a-C can be deposited either via the chemical transport, e.g. in a hydrogen discharge (17-19), by the plasma activated decomposition of hydrocarbons (21-26), or by sputtering and electron beam evaporation onto a cooled substrate (27,28). Chemical transport yields graphitic deposit in agreement with the general rule since the deposition takes place in an intense discharge close to the chemical equilibrium. On the other hand, during the plasma activated decomposition of hydrocarbons, sputtering and electron beam evaporation, the deposition takes place irreversibly, far away from equilibrium, resulting in the formation of metastable a-C. Unlike graphite, such films are hard, transparent, they show a high resistivity, and, upon annealing, they transform into the more stable graphitic form. Table 1 summarizes the properties of these films vis-a-vis the thermodynamically stable graphite and the metastable diamond phase.

The apparent similarity of the properties of a-C and diamond led some researchers to the erroneous conclusion that one is dealing with amorphous diamond. More recent investigations into the properties of a-C (25-28) have shown that the results can be explained in terms of a disordered network of predominantly three-fold coordinated carbon atoms.

TABLE 1: see next page

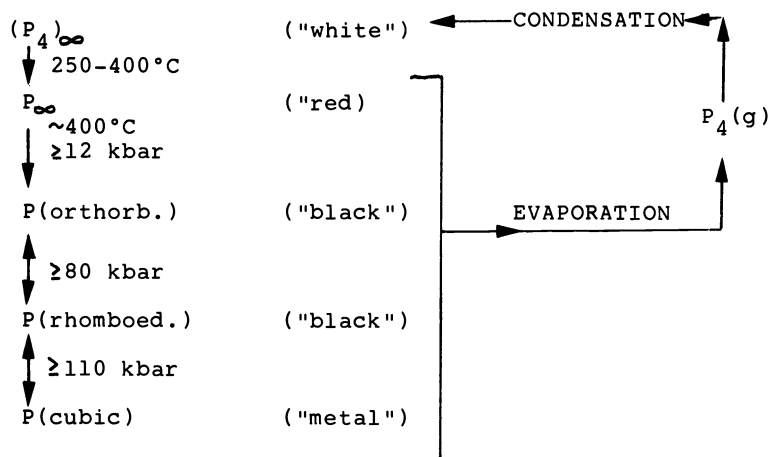
TABLE 1. Comparison of the physical properties of a-C prepared by the plasma activated decomposition of hydrocarbons (diluted with argon) with that of diamond and graphite

	a-C	Diamond	Graphite
HARDNESS (kg/mm ²)	~ 3000	7000	soft
DENSITY (g/cm ³)	1.9-2	3.52	2.26
BANDGAP (eV)	2.8-4	5.6	metal
ELECTRIC CONDUCTIVITY (Ω cm) ⁻¹	10 ⁻⁹ -10 ⁻⁵	$\geq 10^{-18}$	~ 10 ³
DIELECTRIC CONSTANT	1.6-4.9	5.76	metal
INDEX OF REFRACTION	1.8-2	2.42	metal
T _{transf.} (°C)	760	1800	stable
[H] (at %)	10-25	0	0
[Ar] (at %)	several at %	0	0

Amorphous and microcrystalline black phosphorus

Phosphorus is among the elements occurring in a variety of allotropic forms, a simplified summary of which is given in Table 2 (for a summary of the literature see (29-31)).

TABLE 2. Allotropic forms of elemental solid phosphorus (simplified). P(orthorhombic), "black" is the thermodynamically stable modification under standard conditions. The temperature and pressure data indicate the necessary conditions for the transformation. P₄(g) molecules are being formed during evaporation and the metastable, highly reactive "white" phosphorus upon condensation.



Bond angle distortion in the tetrahedral P₄-molecules is the origin of the high reactivity of the "metastable", white phosphorus. Also the more stable, red phosphorus possesses only a limited stability against oxidation in air.

However, annealing at a pressure of ≥ 12 kbar is necessary to obtain the stable, orthorhombic modification.

As shown in our previous papers (20,32-34), phosphorus can be chemically transported in a hydrogen plasma and deposited at temperatures between ~ 8 and 200°C and at deposition rates of up to ≈ 1000 Å/s. Below $\sim 120^\circ\text{C}$, amorphous, remarkably stable and pure phosphorus with a few at % of incorporated hydrogen is obtained (33,34). X-ray photoelectron spectroscopy studies have revealed that its surface remains unoxidized even after long-term exposure to air (humidity $\sim 30\%$) at temperatures up to $\sim 150^\circ\text{C}$ (35). Electrical, optical and some further properties were also studied and are described elsewhere (33, 34,36). These, rather surprising properties became understandable after a study of the radial distribution function revealed a close similarity of the short-range order of this material with that of the stable, "black" modification (31).

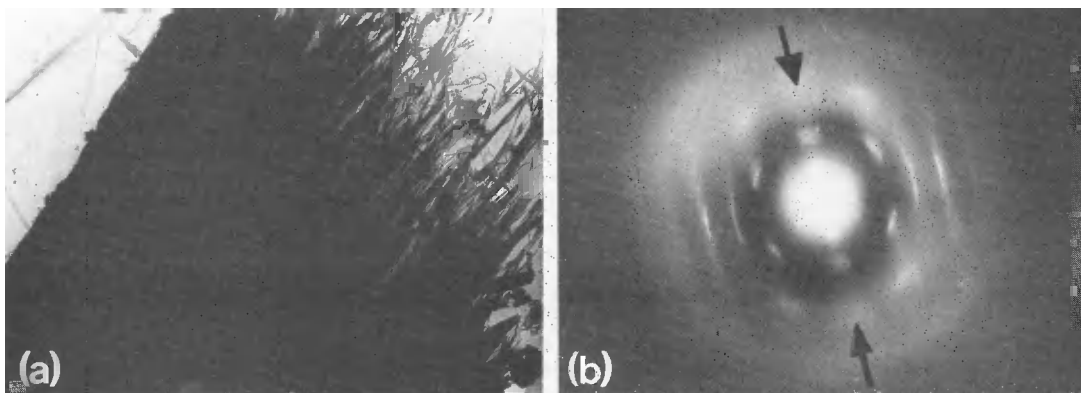


Fig. 1. Microcrystalline, fibrous "black" phosphorus deposited via the chemical transport in hydrogen plasma at $T_d \approx 200^\circ\text{C}$. a: Transmission electron photomicrograph $10'000\times$; b: Electron diffraction pattern with an arrow indicating the orientation perpendicular to the fibre axes.

If the deposition via the chemical transport is performed at a lower rate and higher temperature (e.g. < 100 Å/s and $\geq 180^\circ\text{C}$), microcrystalline, fibrous material is obtained (Fig. 1) (34). From the evaluation of a series of electron diffraction patterns it can be concluded that the stable, orthorhombic modification of "black" phosphorus is formed during chemical transport at ~ 180 - 200°C and ≈ 1 torr. These preparation conditions, when compared with those given in Table 2 (≥ 12 kbar, $\sim 400^\circ\text{C}$) illustrate that the kinetic barrier to the formation of the stable phase can easily be overcome if the deposition takes place in a plasma close to chemical equilibrium.

Amorphous phosphorus nitride

Phosphorus nitride, P_3N_5 is an example of a solid material which is typically obtained in amorphous form. As yet no single crystals were prepared and the crystal structure is unknown. Among the various methods of its preparation, chemical vapour deposition in a low pressure nitrogen plasma yields the best films (for summary of the preparation and properties see (37)). They can be prepared either from a mixture of phosphine and nitrogen or by chemical transport of phosphorus in a nitrogen plasma combined with subsequent deposition of P_3N_5 (38). The former method yields hydrogenated $\text{P}_3\text{N}_5\text{H}_x$, $x \geq 1.3$. Although both, $\text{P}_3\text{N}_5\text{H}_x$ and P_3N_5 have many properties which are similar, the P_3N_5 deposited via chemical transport shows better stability. For example it has the highest density reported so far (2.79 g/cm³) which does not change even after annealing at $\sim 880^\circ\text{C}$ for 2 days (38). The high dielectric strength of the stoichiometric P_3N_5 which amounts to $\geq 10^7$ V/cm is also remarkable. A comparison of the electric properties, which are very sensitive to structural imperfections, of the plasma deposited and conventionally prepared films, shows unambiguously the beneficial effect of the plasma technique, in particular of

of the chemical transport (38).

In summary of this section, the three examples discussed here illustrate the beneficial effect of the plasma on the properties of thin films whenever low deposition temperatures are required. Deposition under conditions close to a reversible chemical equilibrium generally favours the formation of a more stable solid phase. Further examples, to a certain degree less understood in terms of the chemistry, can be given (7,8,20). It depends solely on the criteria given by the particular application whether the more stable (e.g. crystalline) or the metastable (e.g. amorphous) phase is to be preferred. However, the development of science has never been guided solely by the criteria of immediate application of results and in this sense, the utilization of both, reversible and irreversible plasma chemical processes is of great importance to various branches of solid state research. The deposition of silicon, to be discussed in the following section, is an excellent example of the unique combination of basic research with promising applications.

AMORPHOUS AND CRYSTALLINE SILICON

As early as in 1880 Ogier (39) and, later, in 1935 Schwarz and Heinrich (40) reported on the decomposition of silane in a silent discharge, yielding hydrogen and a solid subhydride of composition $\text{SiH}_{1-1.7}$. Later on, several researchers used this technique to prepare various higher, volatile silanes, such as Si_2H_6 , Si_3H_8 , Si_4H_{10} (41-43) and novel compounds, such as H_3GeSiH_3 (41), silylphosphines SiH_3PH_2 , $\text{Si}_2\text{H}_5\text{PH}_2$, and others (42,43). Although seldom mentioned in the more recent publications, these studies represent the precursors of the modern, hectic development in the field of amorphous and polycrystalline silicon.

In 1968, Vepřek and Mareček reported on the preparation of polycrystalline silicon and germanium (referred today as microcrystalline, $\mu\text{c-Si}$ and Ge) by chemical transport in a low pressure hydrogen plasma (44) and in 1969 Chittick, et al published their pioneering paper on the deposition of amorphous silicon (a-Si) by the plasma-activated decomposition of silane (45).

For a long period of time many researchers shared a rather pessimistic opinion regarding the application of a-Si in the fabrication of electronic devices because of the apparent lack of the possibility of influencing its electronic properties by substitutional doping (46). The problem was due to the high density-of-states within the pseudo-gap which prevented any noticeable shift of the Fermi level by doping.

In their systematic study performed between about 1970 and 1975 Spear and Le Comber succeeded in tailoring the deposition conditions of a-Si in order to reach a remarkably low density of states within the pseudo-gap (47,48). This work opened the way towards the successful substitutional doping of a-Si (49, 50) which allowed a change of the room temperature electrical conductivity of a-Si by 10 orders of magnitude.

A straightforward application of this material appeared to be in the fabrication of low-cost solar cells, which was pioneered by Carlson at the RCA laboratories (51,52) and by Spear et al at the University of Dundee (for a review see (53 - 59)). By optimizing the structure of the a-Si based solar cells, an efficiency of $\sim 7.5\%$ has been achieved by Hamakawa's group in spring 1981 (60) and it is expected that similar efficiency can be achieved in large scale industrial production within the next several years. The estimated costs are in the range of US \$ 0.65 per peak watt (61). The maximum efficiency might approach 8-10 % provided a substantial improvement of the properties of the material can be achieved. Large scale industrial production of low cost solar cells with such parameters alone will of course not solve the future energy problems (particularly in Europe) but it can, if successful, represent an important contribution.

With increasing understanding of the physical properties of a-Si the areas of its applications are fast growing. For example, very recently its applications in the fabrication of field-effect transistors for addressable liquid crystal display panels, for image sensors and for logic circuits (62,63) and in vidicon devices (64) have been demonstrated. The apparently inherent drawback of a-Si-based logic circuits is their slower switching time as compared with single crystal Si-based elements (62), but their low costs and the possibility of building three-dimensional arrangements of such circuits will open up wide areas of their applications including also the computer technology.

During the last two years, microcrystalline silicon, $\mu\text{c-Si}$, has received increasing interest (65-76) because of several reasons: First, it represents the intermediate stage between crystalline and amorphous silicon and hence allows fundamental studies of the transition between the crystalline and amorphous phase to be performed. Results of our measurements of the reaction kinetics in the heterogeneous Si/H-system under plasma conditions (70,77-78) enabled us to achieve an excellent control of the deposition conditions and to perform a systematic study of the crystalline-to-amorphous transition (68, 71). Second, the interest in the $\mu\text{c-Si}$ is further motivated by its possible applications in the electronic industry and in the manufacture of a-Si-based solar cells (76). Third, and last, but not least, it has been shown that various silicon materials which were reported to be amorphous, such as Si/F,H and Si/Cl,H, are of microcrystalline nature (72,75).

In contrast to the progress in the understanding of the physical properties and in the applications of a-Si, the knowledge of the plasma parameters and of the chemical processes controlling the deposition of amorphous and crystalline phases is still insufficient and, as a matter of fact, the preparation as reported in many papers resembles "black magic" rather than science. Therefore, in the following part of this paper we shall give a brief summary of our present understanding of the chemistry of this system together with some results of our investigation of the crystalline-to-amorphous transition. The structural, optical and electrical properties will be summarized as well.

The chemistry of the heterogeneous system Si/H under plasma conditions

Under standard conditions, silane is thermodynamically unstable (cf. reaction (4) (79))

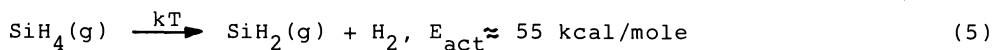


$$\Delta F_{298}^\circ = 13.2 \text{ kcal/mole}$$

$$\log K_p (298 \text{ K}) = -9.7$$

and, if activation energy is provided, it decomposes into solid silicon and molecular hydrogen. In spite of this instability the thermal decomposition proceeds at a practically useful rate only above $\sim 600^\circ\text{C}$. Even at temperatures close to 1000°C the reaction probability for SiH_4 molecules impinging on the silicon surface amounts only to a few percent (80).

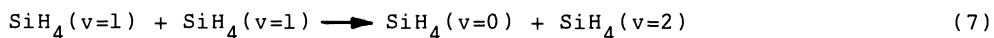
The first step in the gas phase decomposition at $T \lesssim 430^\circ\text{C}$ is dominated by reaction (5)



whereas the radical mechanism (6)



seems to be significant only on the surface (81). The silane decomposition can be activated by UV light (82,83) or, more conveniently, by photosensitization via $^3\text{P}_1\text{Hg}$ states (84-87). More recently, Deutsch (88) has shown that silane can also be decomposed by a multiphonon absorption of IR radiation from a CO_2 - TEA laser. More than 100 photons of energy of $\sim 0.12 \text{ eV}$ ($\lambda = 10.6 \mu\text{m}$) are necessary per each decomposed molecule and the collisional v-v pumping, (7)



appears to be an important energy transfer process involved in the dissociation, which proceeds predominantly via the molecular channel, react. (5).

Although all these methods yield more or less hydrogenated, amorphous silicon, the most convenient and versatile is the activation of the silane decomposition by an electric discharge, as pioneered by Ogier in 1880 (39). In addition, the application of an intense hydrogen plasma with an appreciable degree of dissociation enables reaction (4) to proceed reversibly also from the left hand side to the right, as apparent from the free energy of reaction (8) (79):



$$\Delta F_{298}^\circ = -181 \text{ kcal/mole}$$

Niki and Mains (86) were probably the first to notice a possible reaction of solid monosilane with hydrogen atoms. The expected reversibility of the overall reaction (9)



($m = 1$ for the forward reaction, see eq. (8), and $m = 2$ for the reverse one, see eq. (4) and further below) formed the basis for our earlier experiments on the chemical transport of silicon (and by analogy also of germanium) in a hydrogen discharge.

The exothermicity of reaction (8) implies that it may proceed under plasma conditions but only kinetic data can yield the information regarding the reaction probability and its dependence on the plasma parameters (89,90). Before discussing the kinetics let us point out that since the formation of SiH_3 and possibly SiH_2 should also be exothermic with atomic hydrogen these species must, together with SiH_4 , be considered as possible primary reaction products under plasma conditions where sufficient vibrational excitation can be provided to the surface adsorbed species to cause their desorption. On the other hand, only $\text{SiH}_4(g)$ is expected to be formed in the afterglow and with thermally produced H-atoms (91).

Reaction kinetics and the probable mechanism

The temperature dependence of the rate of the forward reaction (9), i.e.



in a low pressure hydrogen discharge has been measured by Webb and Vepřek (77). It displays a pronounced maximum at a temperature between 40–80°C and, at a given temperature, it increases with increasing discharge current. Thus, the chemical transport of silicon can be controlled by the temperature of the substrate, and/or of the Si-charge, as well as by the discharge current. Accordingly, the transport direction is

$$T_1 \longrightarrow T_2, \quad \mathcal{E}_2 = \mathcal{E}_1 \quad (11a)$$

and

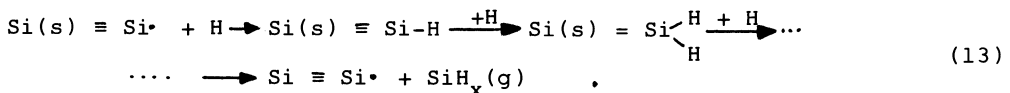
$$\mathcal{E}_2 \longrightarrow \mathcal{E}_1, \quad T_1 = T_2 \quad (11b)$$

where $T_1 < T_2$ are the temperature of the charge and substrate, respectively and $\mathcal{E}_2 > \mathcal{E}_1$ are the plasma densities (e.g. discharge current) at the charge and at the substrate respectively. Also the existence of a reversible chemical equilibrium in this system has been demonstrated in our earlier paper (77,78). It corresponds to a state in which the non-zero rates of the forward and reverse reactions (9) are equal, i.e.

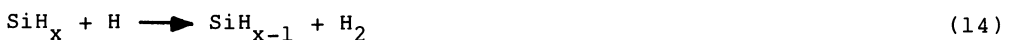
$$\bar{r} = \underline{r}; \quad \bar{r}, \underline{r} \neq 0 \quad (12)$$

In the framework of general non-equilibrium thermodynamics (92) it means that the chemical fluxes vanish but energy fluxes are non-zero (90,93).

Figure 2a shows schematically the experimental arrangement and the control of silicon etching and desposition by temperature of the charge and of the substrate. Figure 2b applies for conditions far on the left hand side of react. (9), i.e. for etching (react. (10)) and one notices that etch rates of more than 15 Å/s were achieved (77) (floating potential, no sputtering). From the measured primary fluxes of positive ions and neutral atoms to the surface it was concluded that the etching is due to neutral H-atoms (70), and the most probable mechanism is the step-wise addition of hydrogen to the surface Si-atoms:



The reverse reaction (9) is essentially the hydrogen recombination (77)



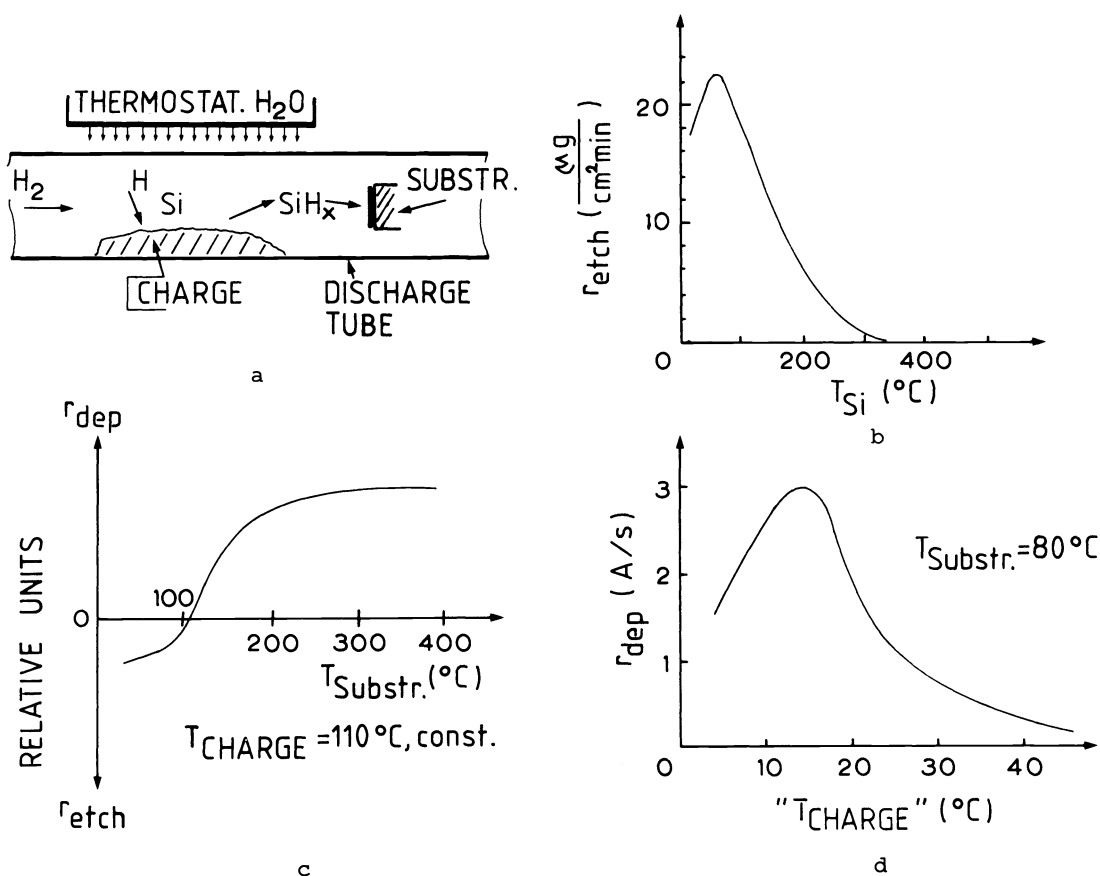
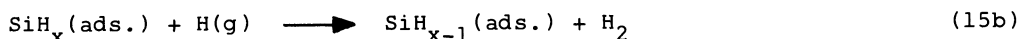
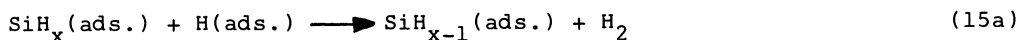


Fig. 2. Control of the chemical transport of silicon in a hydrogen plasma by the temperature of the charge, T_{ch} , and of the substrate, T_s . a) Experimental arrangement b) Dependence of the forward reaction rate on temperature, $p = 0.13$ mbar, $i = 360$ mA, discharge tube radius = 2.5 cm (77) c) Dependence of the deposition-, $r_{dep} = \bar{r} - \underline{r}$, and etching rate, r_{etch} , on the substrate temperature for a constant T_{charge} d) Dependence of the deposition rate on the temperature of charge, T_{ch} , at a constant substrate temperature. Here, " T_{ch} " is the temperature of the thermostated water soaking the outer wall of the discharge tube; the actual T_{ch} is somewhat higher because of the not well defined temperature gradients in the powder Si charge. A similar trend of the curves in Fig. b and d is evident.

By analogy with other systems this process is expected to be fast in the gas phase (comparable to hydrocarbons) (94 - 96) having a rather small activation energy. On the surface, both, the L.-H. and E.-R. mechanisms are feasible (reacts. (15))



and they are expected to have a higher activation energy than reaction (13) (96). There are several studies on the chemisorption of hydrogen on silicon surfaces (for a review see (97)) but, unfortunately, none of them provides conclusive kinetic data. They basically confirm the results of Fig. 2b showing that the chemisorption of H-atoms takes place already at room temperature (98-100) and that silicon is being etched by thermally produced atomic hydrogen (101,102). In more recent work Wagner and co-workers have obtained results giving strong support for the L.-H. mechanism (15a) to take place at tempera-

tures above $\sim 100^\circ\text{C}$ (101,102). Using the high resolution electron energy loss spectroscopy they observed that, starting with the "monohydride" surface phase $\text{SiH}(\text{ads.})$, the $\text{SiH}_2(\text{ads.})$ -groups are formed as intermediates during the formation and desorption of H_2 . The recombination (15a) can also involve a weakly bonded $\text{H}(\text{ads.})$, existence of which was pointed out by Sakurai and Hagstrum (99).

Obviously, our present understanding of the hydrogenated Si-surface is insufficient (103) to give an unambiguous, detailed mechanism of the recombination but the overall picture of chemical transport seems to be well understood: In the charge zone kept at a temperature $T_1 \approx 40\text{--}80^\circ\text{C}$, the forward reaction (13) dominates whereas the heterogeneous recombination (15) which, due to its higher activation energy, leads to the decrease of the surface coverage by chemisorbed hydrogen at higher temperatures, T_2 , dominates at the substrate. Similarly, a higher degree of dissociation of the gas phase hydrogen has the effect of increasing, at a constant temperature, the surface density of chemisorbed hydrogen and, thus, enhancing the rate of the forward reaction (13) (77). Consequently, isothermal transport can proceed in a gradient of the "plasma density" according to eq. (11b).

Effect of bias

Let us now turn to the effect of the substrate bias on the deposition rate (70,104). For this kind of study we used a D.C. discharge in which the substrate can be controllably biased either positively or negatively with respect to the plasma (only the region of negative bias is accessible in an R.F. discharge). If, except for the (electrically conductive) substrate, the whole substrate holder is electrically insulated from the plasma, its current-voltage characteristic can provide the reference "wall potential", V_w , (also called "floating") of the plasma at the position of the substrate. This is illustrated in Fig. 3 which essentially resembles the Langmuir characteristic of a single probe. Figure 4 shows, for comparison, the dependence of the deposition rate on the bias.

At a floating potential, $V_b = 0$, the deposition rate of $\sim 40 \text{ \AA}/\text{min}$ or 3.3×10^{14} Si-atoms/cm²sec may be due to positive ions since their flux of $i_0 = 0.1 \text{ mA}$ which corresponds to $\sim 4 \times 10^{14}$ ions/cm²sec can account for the deposition rate assuming a sticking coefficient of ~ 1 . Drevillon, et al (105) argued for the latter and there is ample evidence that monosilane ions SiH^+ (mainly SiH_2^+) are dominant and disilane ions are the much less abundant ionic species in such plasmas (105-108). However, with increasing negative bias of the substrate the increase in the deposition rate does not follow the ion current suggesting rather a sticking probability of less than 0.2 (cf. Figs. 3 and 4). Although a decrease of the sticking probability with increasing ion energy is to be expected (109) and accounting for the fact that, at the floating potential, the kinetic energy of the ions impinging on the surface amounts to $\sim 5\text{--}10 \text{ eV}$, such a sudden decrease of the ion energy, as well as the overall shape of the curve in Fig. 4 indicate that a purely ionic mechanism of the deposition is an oversimplified picture. In addition, electrically neutral silane radicals are orders of magnitude more abundant than their ionic counterparts and their sticking probability (which to our knowledge has not been measured yet) is unlikely to be correspondingly low.

Further, in the region of the positive bias (see Figs. 3 and 4) electron impact-induced processes have to be considered as well. For example, Ashby and Rye (110) performed experiments showing the strong effect of electron impact-induced processes in enhancing the etch rate of carbon by molecular hydrogen. In a study being presently done at our laboratory evidence for the electron-impact induced etching of silicon under the positive bias has been found (104). Finally, information on the relative extent of ion-backscattering, -implantation, ion-induced sputtering and desorption as a function of their, yet unknown, impinging energy (in the most inconvenient range of 5-100 eV) is required as well.

In summary, the results obtained so far show that the main channel for the hydrogen desorption is the (temperature dependent) reaction (14) and that the deposition rate is strongly influenced by a positive bias of the probe but relatively much less by a negative one. This points to the important rôle of the charged species but more data are needed for a detailed understanding of these processes. These problems are presently under detailed investigation in our laboratory.

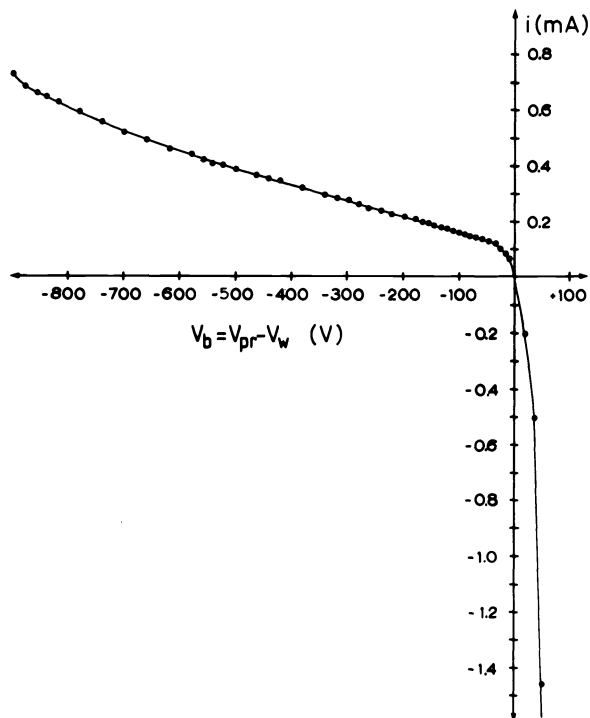


Fig. 3. The current/voltage characteristic of the substrate used as a Langmuir single probe. V_{pr} and V_w mean the potential of the probe and "wall", respectively. Discharge parameters: $p = 0.7$ mbar, $i_{disch} = 126$ mA, discharge tube radius 2.5 cm, effective substrate area ~ 1.5 cm², $T_{dep} = 260^\circ\text{C}$

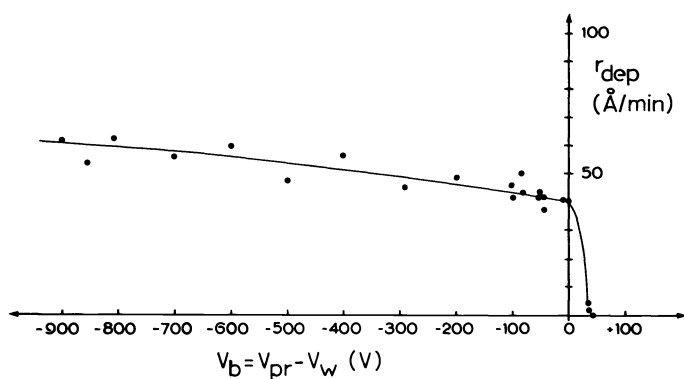


Fig. 4. Dependence of the deposition rate, r_{dep} , on the bias, $V_b = V_{pr} - V_w$. Discharge parameter as given in Fig. 3.

Parameters controlling the formation of amorphous and polycrystalline silicon

In the past, the question was raised as to why one obtains in one case amorphous and in another situation crystalline silicon, although the plasma conditions are rather similar. Recently we have shown that the decisive parameter controlling the structural properties of the deposit is the departure of the system from chemical equilibrium (70). This is consistent with the well known experience of chemists and crystal growers that growth in the vicinity of an equilibrium state (sublimation, chemical transport, solution growth, etc) favours the formation of a well ordered, stable solid phase. Basically, there are two effects involved:

a) The Ostwald's law of stages which reflects the fact that the formation of nuclei of the stable, crystalline phase usually requires a higher activation energy than the formation of the nuclei of the metastable, amorphous phase (111). The reason being that the most stable structure of small clusters, which is basically governed by the minimization of their surface energy, is generally incompatible with the structure of the stable crystal lattice (112-118). The problem is related to the third peak in the radial distribution function which reflects the change in the bond topology of a-Si as compared to the diamond lattice of c-Si (46,119).

The minimization of the surface energy is essentially equivalent to maximizing the number of Si-Si bonds for a cluster of a given size (or, alternatively, to minimizing the number of dangling bonds at the surface). Building of models (112-114) and theoretical calculations (116-118) have shown that this condition is met by amorphonic structures such as regular icosaedron, pentagonal dodecaedron, and others. Obviously, a high activation energy is necessary to break the bonds and transform such a cluster into a nucleus of a stable, crystalline phase. This energy can be easily provided if the deposition takes place close to an equilibrium state, but not during quenching far away from equilibrium.

b) The mineralization effect which, in the case of a heterogeneous solid-gas system, essentially involves chemical transport in a gradient of free energy arising between solid particles of different sizes (120). Consider a reversible heterogeneous reaction (16) in which, under given conditions, chemical equilibrium



is established with $|\log K_p| \leq 3$ (K_p is the equilibrium constant). The free energy of small solid nuclei is larger than that of the large ones because of the excess term due to the surface energy, i.e.

$$\Delta F^\circ[A(\text{small nucl.})] > \Delta F^\circ[A(\text{large nucl.})] \quad (17)$$

and, consequently,

$$\log K_p(\text{small nucl.}) > \log K_p(\text{large nucl.}) \quad (18)$$

As a result, isothermal chemical transport takes place between nuclei of different size, the larger growing at the expenses of the smaller ones. Similar transport will take place also during sublimation, solution growth and in the case when nuclei of both the metastable (e.g. amorphous) and stable (e.g. crystalline) phases are present in the system provided that the deposition takes place in the vicinity of an equilibrium state where both, the forward and reverse reaction rates are non-zero (i.e. $r_{\text{dep}} = \bar{r} - \underline{r}$, $\underline{r} \gg \bar{r}_{\text{dep}}$).

Now, the question arises as to how these rules apply to the deposition of silicon in a Si/H-plasma. We have shown in the previous section that a reversible chemical equilibrium can be established in this system. At low deposition temperatures (e.g. $T_d \leq 250^\circ\text{C}$) the etch rate is appreciable (Fig. 2b) and the mineralization effect is expected to contribute significantly to the structural ordering of the growing film, enabling the deposition of $\mu\text{c-Si}$ essentially free of any amorphous phase (except for the grain boundaries), at a temperature of $\sim 65^\circ\text{C}$ (67,71). As yet, it is not clear as to what extent this effect influences the growth of the films at $T_d \geq 300^\circ\text{C}$ where the measured etch rate apparently approaches zero (see Fig. 2b and (77)). However, the reported measurements of the etch rate were performed with a single crystal Si chip (77) whereas the hydrogenated amorphous films are much more reactive (121) even above 300°C . Possibly other processes, such as recombination on the surface can also enhance the surface mobility of the monomers, thus giving rise to the same effect, but the fact that the crystallite size approaches a quasi-limiting value of $\sim 150 \text{ \AA}$ at $T_d \approx 300\text{-}450^\circ\text{C}$ (Fig. 5) suggests the former process to be most important. Further increase in the crystallite size is to be expected only around the recrystallization temperature, i.e. around $\sim 800^\circ\text{C}$ (see also (122)).

In a previous paper we have shown that, at a typical deposition rate of $\sim 1 \text{ \AA}/\text{sec}$, up to several thousand H-H recombination events take place on the surface per deposited Si-atom and energy of $\beta E_{\text{diss}} \approx 0.5\text{-}1 \text{ eV}$ is dissipated into the film per each H_2 -formed (70). In view of the lack of experimental data on the recombination- and energy accommodation coefficient (γ and β , respectively) for hydrogen atoms on Si, this estimate was based on the measured degree of dissociation and on the γ and β values estimated from the correlations given by Melin and Madix (123). Since the energy quantum of $\sim 0.5\text{-}1 \text{ eV}$ is much higher than the Debye cut-off energy, $k\theta$ (k - Boltzmann constant, θ - Debye temperature) and because of the localized nature of the recombination process, highly energetic short wave length phonons of the solid are likely to be excited. Their thermalization, which takes place via phonon-phonon interactions, is a relatively slow process. Thus, the nuclei formed on the surface during growth are non-thermally excited to higher vibrational states. Such an excitation is likely to induce their transformation into the stable, crystalline structure. Further research work is necessary in order to obtain a deeper

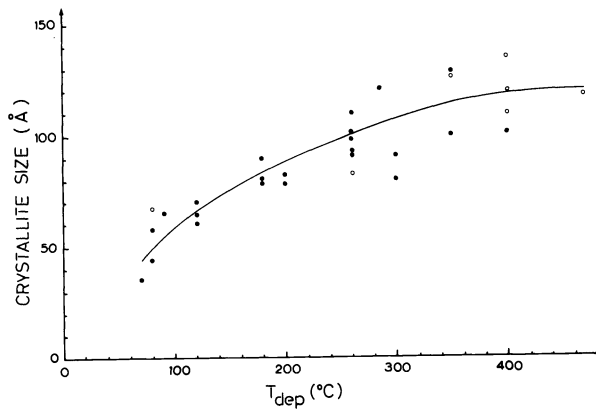


Fig. 5. Measured dependence of the crystallite size of $\mu\text{c-Si}$ on the deposition temperature.

insight into the mechanism of this transformation. The recent theoretical work of Dandolo, et al (124-126) and the thermodynamic theory of the crystalline-to-amorphous transition (68) represent the first steps into this direction.

The decreasing etch rate with increasing temperature above $\sim 80^\circ\text{C}$ (Fig. 2b and (77,78)), the results of Wagner, et al (101-102), and the results of an analogous C/H-system where conclusive experimental data are available (96) indicate that the recombination coefficient of hydrogen on Si decreases with decreasing temperature. This could explain why, under given discharge conditions, a lower limit of deposition temperature at which $\mu\text{c-Si}$ can be grown apparently exists (e.g. $\sim 65^\circ\text{C}$ under conditions mentioned above), although the etching rate (i.e. the mineralization effect) is rather high. As in the case discussed previously, more experimental data are required.

Comparison of the deposition conditions for $\mu\text{c-Si}$ and a-Si: Departure of the system from chemical equilibrium

Consider again reaction (9). Starting from a non-equilibrium state $\bar{r} \neq r$, chemical equilibrium is approached at a rate characterized by the relaxation time τ which, in general, depends on the reaction mechanism and concentrations of the reactants. Since, as yet, this functional dependence is unknown we define a characteristic time τ by eqs. (19a) and (19b) when starting from the left and right hand side of reaction (9), respectively:

$$[\text{SiH}_x]_\tau = [\text{SiH}_x]_{t \rightarrow \infty} (1 - e^{-1}) \quad (19a)$$

$$[\text{SiH}_x]_\tau = ([\text{SiH}_x]_{t=0} - [\text{SiH}_x]_{t \rightarrow \infty}) \cdot e^{-1} \quad (19b)$$

Here, $[\text{SiH}_x]_\tau$ is the concentration of the SiH_x species at time τ , t_{res} is the residence time of hydrogen and SiH_4 molecules, respectively in the discharge between the gas inlet and the observation point; the remaining symbols are self-explanatory. For the purpose of the present discussion we consider only the dependence of τ on discharge current density at the typical pressure and temperature used for the deposition of good quality films, shown in Fig. 6. The measurements were performed using the collisionless extraction technique combined with mass spectrometric detection (121). One sees that with increasing discharge current density, τ decreases reaching a value of a few tenths of a sec, and that hydrogenated, amorphous silicon reacts noticeably faster than polycrystalline material. The decomposition of silane in a weak discharge with a current density of $\approx 1 \text{ mA/cm}^2$ (resp. a "power density" of $\leq 0.01 \text{ W/cm}^3$) is, however, characterized by $\tau \geq 10 \text{ sec}$.

Table 3 summarizes the typical conditions for deposition of a-Si and $\mu\text{c-Si}$, the latter by chemical transport and by the "high power" discharge in silane diluted with hydrogen [75,76].

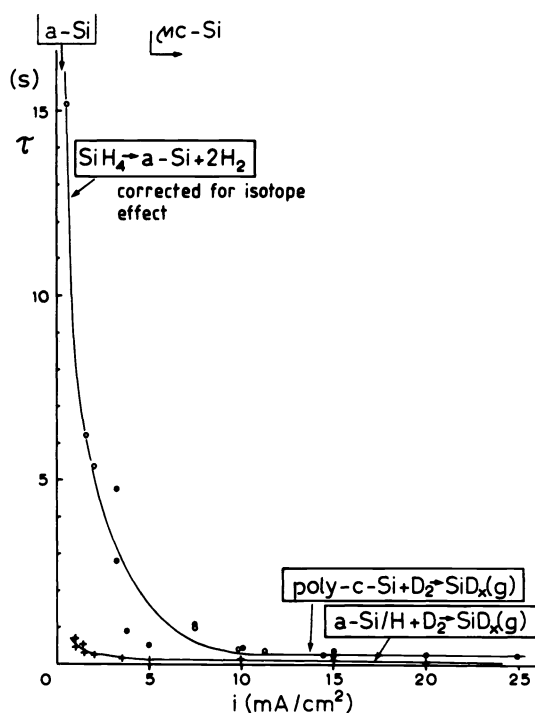


Fig. 6. Dependence of the characteristic time of reaction (9) on discharge current density (70,121). $p \sim 0.84$ torr, $T \sim 200^\circ\text{C}$. The density of electric power dissipated in the plasma is approximately obtained by multiplying the current density by the axial field strength of about 10 to 20 V/cm.

TABLE 3. Comparison of discharge parameters for the deposition of a-Si and $\mu\text{c-Si}$. *) Equilibrium composition as measured by mass spectrometry (121).

Deposit (method)	Feed gas (vol.%)	Power density (W/cm^3)	t_{res} (sec)	τ (sec)	t_{res}/τ
$\mu\text{c-Si}$ (chem.transp.)	$\geq 99\% \text{ H}_2 + \text{H}^*$ $\leq 1\% \sum \text{SiH}_x$	≤ 0.1	≥ 5	0.2-0.5	≥ 10
$\mu\text{c-Si}$ "high power"	$\geq 97\% \text{ H}_2$ $\leq 3\% \text{ SiH}_4$	≥ 0.1	≥ 2.5	0.2-0.4	≥ 8
a-Si	SiH_4 (+Ar, ...?)	≤ 0.01 < 0.001	0.1 1-5	> 1 > 20	≤ 0.1 < 0.25

From the data given in the table we conclude that:

- The deposition of $\mu\text{c-Si}$ takes place under conditions close to chemical equilibrium regardless of the method used.
- a-Si is obtained if the deposition takes place far away from chemical equilibrium where only a small amount of power is dissipated into the surface of the growing film (see Fig. 6). c) Thus, the structural properties are controlled by the general rules as outlined above.

Of particular interest is the equivalence of the "high power" method (75) and chemical transport. Diluting silane with hydrogen and application of higher

power density at a relatively small flow rate provides conditions which are automatically reached if one starts, as in the case of chemical transport, from solid silicon and hydrogen. The obvious advantage of the latter method is the fact that no silane is needed. However, chemical equilibrium is obtained also when starting from pure silane provided conditions are chosen such, that t_{res}/τ is large. This is illustrated by Fig. 7 which shows the dependence of the silane concentration in the plasma on residence time, t_{res} , when starting either from silane (upper curve) or from solid silicon and hydrogen (lower curve). One sees that the concentration of silane, which is the dominant gaseous species, approaches the same value within experimental error when the system approaches chemical equilibrium (for further details see (121)).

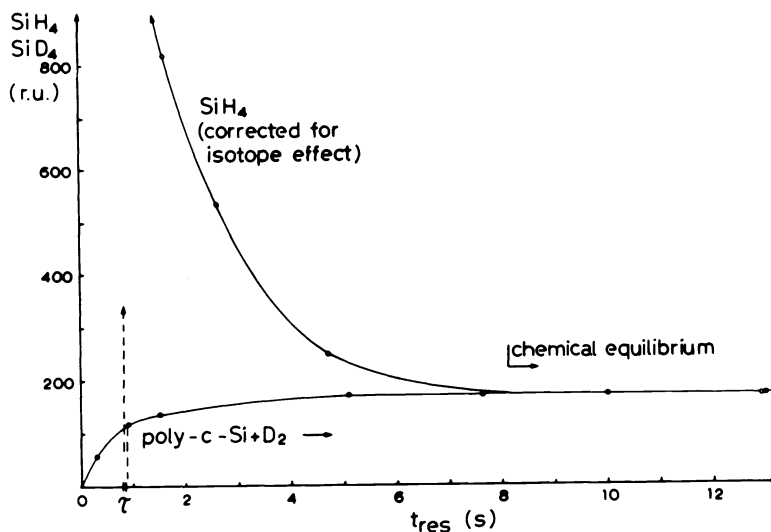
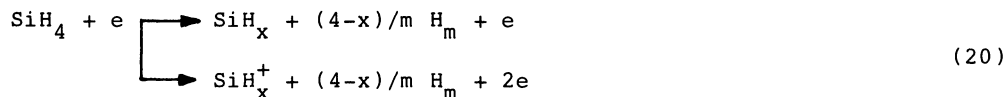


Fig. 7. Dependence of the steady state concentration of silane on the residence time. $p \approx 0.55$ torr, $i = 7.5$ mA/cm², $T \approx 210^\circ$ C. The chemical equilibrium concentration of silane in the gas phase is independent of the initial composition.

In contrast to the relatively consistent picture of the formation of μ C-Si the mechanism of the deposition of good quality a-Si is still lacking. Much work has been done on the decomposition of silane in low pressure plasmas (105-108, 127-129) and a certain understanding of the electron impact processes and of the ion-molecule reactions has been achieved, but very little attention has been devoted to the possible rôle of the vibrational excitation processes, which are known to dominate the dissociation in many gases under plasma conditions (130) and to the processes taking place at the surface of the growing film. One of the problems making the understanding of this system difficult is the inadequate characterization of the discharges being used by different groups. Thus, based on numerous discussions with friends working in this field rather than on the published data, we arrived at the following approximate picture: Since the sticking coefficient of SiH₄ is very low (80), the first step must be either the electron impact-induced dissociation in the gas phase



as discussed by Nolet (127) and Turban, et al (106,107), or the ion impact-induced dissociation and chemisorption on the surface



The importance of the latter process is substantiated by the examples discussed by Winters (91). The neutral or ionic species are then chemisorbed (the

latter undergo Auger recombination (131)) on the surface of the growing film where further decomposition takes place. The results of Drevillon, et al suggest that there is a correlation between the deposition rate and the substrate bias indicating the importance of ion-bombardment in the growth process, but it is not clear if the ions are just dominating the particle flux determining the chemisorption rate or if they rather take part in the decomposition processes as indicated by eq. 21 (see also the above discussion regarding $\mu\text{c-Si}$). It has been realized already by Spear, et al that in order to obtain stable, good quality films the surface of the growing film must be in "contact with the discharge" (132,133). Further results in support of the importance of surface processes were given by Knights, et al (134-136) who have shown the effect of the negative bias of the substrate and of the nature of the inert gases used to dilute the silane, on the homogeneity and defect density of the deposited films. Evidently, isotropic films with a low density of defect and a reasonably low hydrogen content (e.g. ≤ 10 at % for $T_d \approx 260^\circ\text{C}$) are obtained by an appropriate balance of the surface processes during the deposition as achieved by several groups on an empirical basis. Thus, future research has to be directed towards these processes taking place under conditions far away from chemical equilibrium ($t_{res} \ll \tau$, see Table 3).

Based on the comparison of the properties of a-Si as reported by various groups and their apparatus for deposition, and by analogy with numerous data obtained with different systems I arrived at the conclusion that the decisive rôle of ion bombardment is the ion impact-induced chemisorption (eq. (21)) which has to be dominant over the process in the gas phase (eq. (20)) in order to obtain good quality a-Si films. Furthermore, certain amount of ion bombardment has a beneficial effect on the structural ordering of the film but the ion energy must not exceed a certain critical value to avoid radiation damage of the deposited film. Our data suggest that a negative bias of about 100 to 200 V at a pressure of ~ 0.2 to 1 torr provides the best conditions. At the moment, this should be regarded as a suggestion which needs verification by appropriate experiments.

PROPERTIES OF MICROCRYSTALLINE SILICON

In this section we shall briefly summarize some properties of microcrystalline silicon deposited in the plasma. A discussion of the properties of a-Si is beyond the scope of this paper and we therefore refer to the literature (46, 137), and in particular to the excellent review by Fritzsche (138).

The crystalline-to-amorphous transition

The knowledge of the kinetics of reaction (9) allowed us to achieve an excellent control of the deposition and prepare films of a well defined crystallite size between ~ 150 and 30 \AA (see Fig. 5), but not below the latter value for films deposited at a floating potential. The lower limit of the crystallite size could be extended to $\sim 20 \text{ \AA}$ by depositing under negative bias in excess of -200 V when compressive stress is built up in the films due to ion-implantation (68,69).

Measurement of the lattice constant of $\mu\text{c-Si}$ films revealed a lattice dilatation below a crystallite size of $\sim 100 \text{ \AA}$, which increases with decreasing crystallite size reaching ~ 1 to 1.2% for the lower limit of $\sim 30 \text{ \AA}$. Although no microscopic interpretation has yet been attempted there is little doubt that the dilatation is due to the increasing contribution of the surface energy of the crystallites with decreasing crystallite size and is related to the reconstruction of their surfaces. Consequently, the elastic energy associated with this dilatation represents a destabilizing, excess term

$$\delta F(\mu\text{c-Si}) = \frac{9}{2} v_{\text{mole}} \cdot B \cdot \left(\frac{\Delta d}{d_0}\right)^2 \quad (22)$$

in the free energy of $\mu\text{c-Si}$ (v_{mole} , B and $\Delta d/d_0$ mean the molar volume, bulk modulus and the linear dilatation of the lattice, respectively). In the limit of $\Delta d/d_0 \sim 1 \%$ this term equals the excess free energy of a-Si:

$$\delta F(\mu\text{c-Si}) = \delta F(\text{a-Si}) \quad (23)$$

Equation (23) represents the thermodynamic criterion for a phase transition. In the case of silicon, where the bond topology is different in c-Si and a-Si, one deals with a discontinuous order-disorder transition. The theoretical aspects and experimental evidence for the discontinuous nature of this transi-

tion have been summarized in our recent paper (68).

Structural properties and hydrogen content

It is well known that impurities can induce crystallization by lowering the activation energy for nucleation. (E.g. the recrystallization of aged glasses, effect of alkali elements on the recrystallization of silica, and of TiO₂ and ZrO₂ in modern glass ceramics (139,140)) and similar effects have been observed in heavily doped silicon (73,75). In such cases, materials are obtained in which the crystallites are imbedded in an amorphous matrix.

The X-ray diffraction of the μ c-Si deposited via the chemical transport shows no sign of such an amorphous component (66). This conclusion is further supported by a comparison of the relative intensity of Raman scattering from μ c-Si attributed to a surface-like mode with the relative number of Si-atoms localized at the grain boundaries as evaluated from the crystallite size and with the hydrogen content which, for a given crystallite size, give nearly equal values (see Table 4 and (67,71)).

TABLE 4. Comparison of the relative number of surface atoms, N_s/N_{total} , calculated from the measured crystallite size with the hydrogen content and with the relative intensity of the Raman scattering from the grain boundaries, I_s/I_c , calculated from the measured intensities and accounting for the relative values of the scattering cross sections (see (71) for details).

Crystallite size (Å)	N_s/N_{total} (%)	H-content (at. %)	I_s/I_c (%)
35	24	≥ 12	15.2
48	17.5	≥ 12	14.1
58	14.5	~ 12	9.1
72	11.7	~ 7	5.1
83	10.1	~ 4	3.1
98	8.6	~ 1	3.1
130	6.5	≤ 1	2.1

The hydrogen content and thermal evolution resemble closely those of a-Si, but from the infra-red absorption spectra which shows well resolved, sharp peaks in the region of the SiH₂ and SiH₃ stretching region we concluded that these species are localized at the grain boundaries (66).

Of a particular interest is the preferential orientation of the crystallites with respect to the surface of the substrate observed at low and high deposition temperatures (Fig. 8). Below $\approx 150^\circ\text{C}$ the films show preferential orientation of the (111) planes parallel to the substrate, above $\approx 250^\circ\text{C}$ increasing preferential orientation of (110) parallel to the substrate is found indicating that completely oriented films should be obtained at $T_d \approx 500^\circ\text{C}$. The effect is independent of the nature of the substrate (silica glass, metallic glasses, polycrystalline aluminum, molybdenum and stainless steel foils, sapphire and silicon single crystals) and, thus, related to the mechanism of the deposition process, in particular to that of the hydrogen recombination.

Optical absorption

The absorption coefficient, α , measured between ~ 0.5 and 3 eV exceeds that of single c-Si and, in some cases even that of a-Si and it does not show any significant change upon annealing in UHV at 650-800°C (66). At a given photon energy, α increases with increasing deposition temperature reaching a maximum at $T_d \approx 350^\circ$ and it decreases at even higher T_d . Richter and Ley, who recently also found enhanced absorption in similar samples, have pointed out that it cannot be explained in terms of a relaxation of the k-vector selection rule (141). Our more recent results indicate that the higher absorption arises due to a combined effect of surface morphology, internal scattering on grain boundaries and of absorption by structural defects associated with the grain boundaries (142).

Of interest is also the measurement of Tsu, et al, showing that the absorption

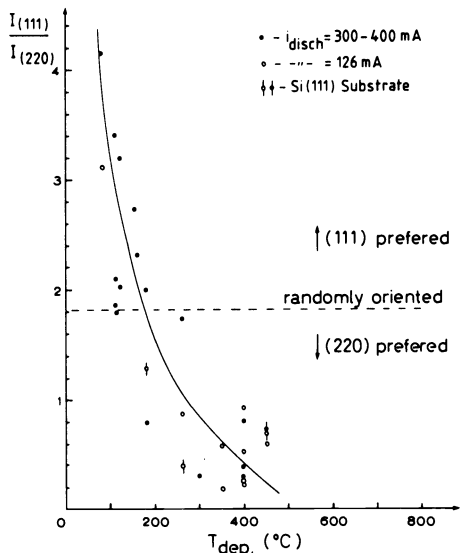


Fig. 8

Fig. 8. Dependence of the intensity ratio of the (111) and (220) X-ray diffraction peaks on the deposition temperature for samples deposited in two different apparatus at pressure varying between ~ 0.1 and 1 torr, discharge current ~ 126 and 400 mA (discharge tube diameter ~ 5 cm). Silica glass, metallic glasses, polycrystalline Al, Mo and stainless steel foils, and single crystal sapphire and silicon were used as substrates.

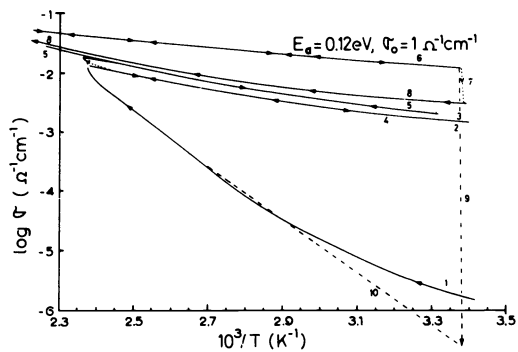


Fig. 9

Fig. 9. Dependence of the logarithm of dark conductivity, $\log \sigma$, on the inverse temperature, $10^3/T$, illustrating the effect of contamination by air and by oxygen: curve 1: first heating up under vacuum better than 8×10^{-6} torr after a long term exposure of the sample to air; curves 2 to 5: repeated cycling between 20 and 150°C with a ~ 15 min annealing at 150°C, followed by ~ 2 hr annealing at $\approx 220^\circ\text{C}$ (curve 5) and cooling down to 20°C (curve 6); curve 6: repeated cycling between 20°C and 220°C under vacuum better than 1×10^{-6} torr; curve 7: sample stored under vacuum for ~ 24 hr, followed by heating up to 220°C (curve 8) and cooling down (again along curve 6). Curve 9: exposure to oxygen at a pressure chosen between ~ 1 and 100 torr; curve 10: heating up to $\approx 220^\circ\text{C}$ under vacuum; after annealing at this temperature curve 6 is measured upon cooling again. Sample parameters: $T_d = 265^\circ\text{C}$, thickness $1.8 \mu\text{m}$, Al-electrodes in a gap geometry, gap varied between 0.2 and 2 mm; voltage 10-30 V.

at higher energies resembles that of c-Si showing a sharp peak associated with the transition in the [100] direction (143).

Electrical conductivity, electron spin density and oxygen content (144)

In an earlier paper (66) we reported the room temperature conductivity of the $\mu\text{c-Si}$ films to range between $\sim 10^{-10}$ and 10^{-6} (Ωcm) $^{-1}$ for samples deposited at ~ 110 and 260° respectively, with an activation energy of ~ 0.52 - 0.87 eV and observation that annealing under high vacuum results in significant changes of the conductivity. More recently we performed a detailed study extending the range of the deposition temperature up to 450°C . The results of this study can be summarized as follows:

The dark conductivity of the samples shows typically a well-defined exponential dependence $\sigma = \sigma_0 \exp(-E_a/kT)$ with both, σ_0 and E_a depending on T_d and on the contamination of the samples by air constituents, mainly by oxygen. Figure 9 illustrates this effect. Changes of the room temperature conductivity, $\sigma_{R.T.}$, up to seven orders of magnitude have been observed upon the reversible adsorption and desorption of dry oxygen. For the interpretation of any conductivity measurements performed on $\mu\text{c-Si}$ it is important to note that the oxygen desorption takes place with reasonable rate only above $\sim 200^\circ\text{C}$ and it takes up ≈ 10 days for the samples to reach saturation during their exposure to air.

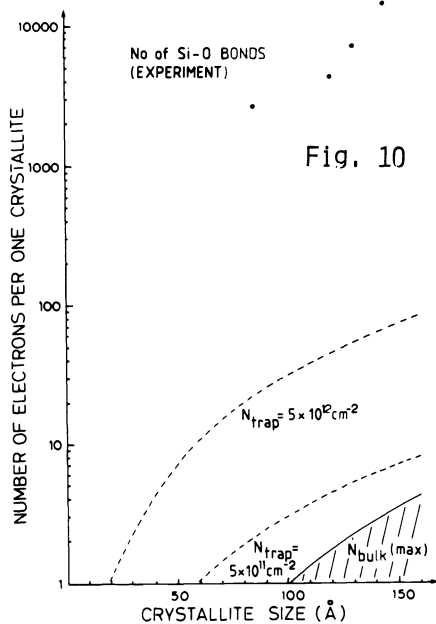


Fig. 10. Comparison of the total number of free electrons in one crystallite, $N_{\text{bulk}}(\text{max})$, with the number of trapping sites on the crystallite surface assuming the trapping sites density of 5×10^{11} and $5 \times 10^{12} \text{ cm}^{-2}$, and with the total number of irreversibly incorporated oxygen.

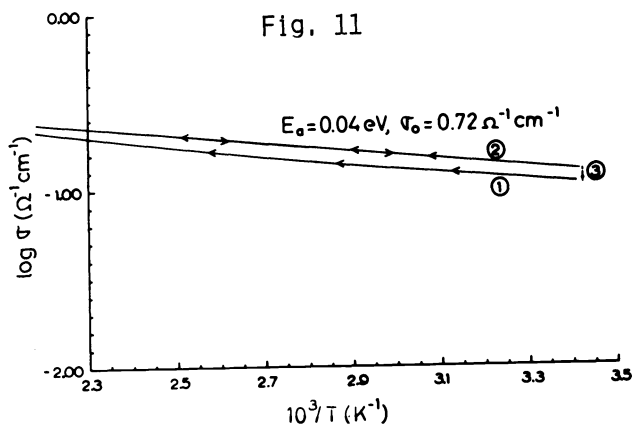


Fig. 11. Dark conductivity versus inverse temperature of a sample deposited at 400°C . Curve 1: first heating up to $\sim 230^\circ\text{C}$; curve 2: cooling down; curve 3: exposure to 100 torr O_2 for several days. During a subsequent annealing under vacuum the conductivity follows curves 1 and 2 again.

Besides this reversible absorption, irreversible incorporation of up to ≈ 10 at % of oxygen with formation of Si-O bond was measured by quantitative infra-red absorption, the saturation being reached only after several weeks. The reversibly adsorbed oxygen cannot be detected by infra-red spectroscopy indicating, together with the reversibility of the process, a non-dissociative nature of the adsorption. Further details and quantitative data are given in our paper to be published.

The measured changes of E_a and σ_0 due to oxygen contamination cannot be interpreted in terms of the grain boundary barrier model (145-147) since the depletion layer extends through the whole grain resulting in an effective shift of the Fermi level. This is illustrated by Fig. 10 which compares the total number of free electrons in one crystallite (the assumed density $n_{\text{el}} \approx 10^{18} \text{ cm}^{-3}$ represents an upper limit (76)) with the number of surface trapping sites (the value of $5 \times 10^{11} \text{ cm}^{-2}$ is a lower limit) and with the amount of irreversibly adsorbed oxygen which provides some measure of the "active surface area".

Behaviour similar to that illustrated by Fig. 9 has been found for most samples deposited at $T_d \approx 260^\circ\text{C}$ and only a careful control of the deposition conditions yielded samples which showed only small changes. An example is shown in Fig. 11. Further details can be found in Ref. (144).

The changes in conductivity are accompanied by changes in the density of electron spins. On the contaminated samples, spin density of the order of 10^{17} cm^{-3} was measured with the $g = 2.0055$ factor usually attributed to "dangling bonds". After annealing under high vacuum, the ESR signal became undetectable and only after exposure of the samples to air the signal appeared again, approaching the original value only after a long period. This reproducible behaviour is illustrated in Fig. 12. Figure 13 shows the dependence of the electron spin density on the time of exposure of the sample to air (see (144) for further details).

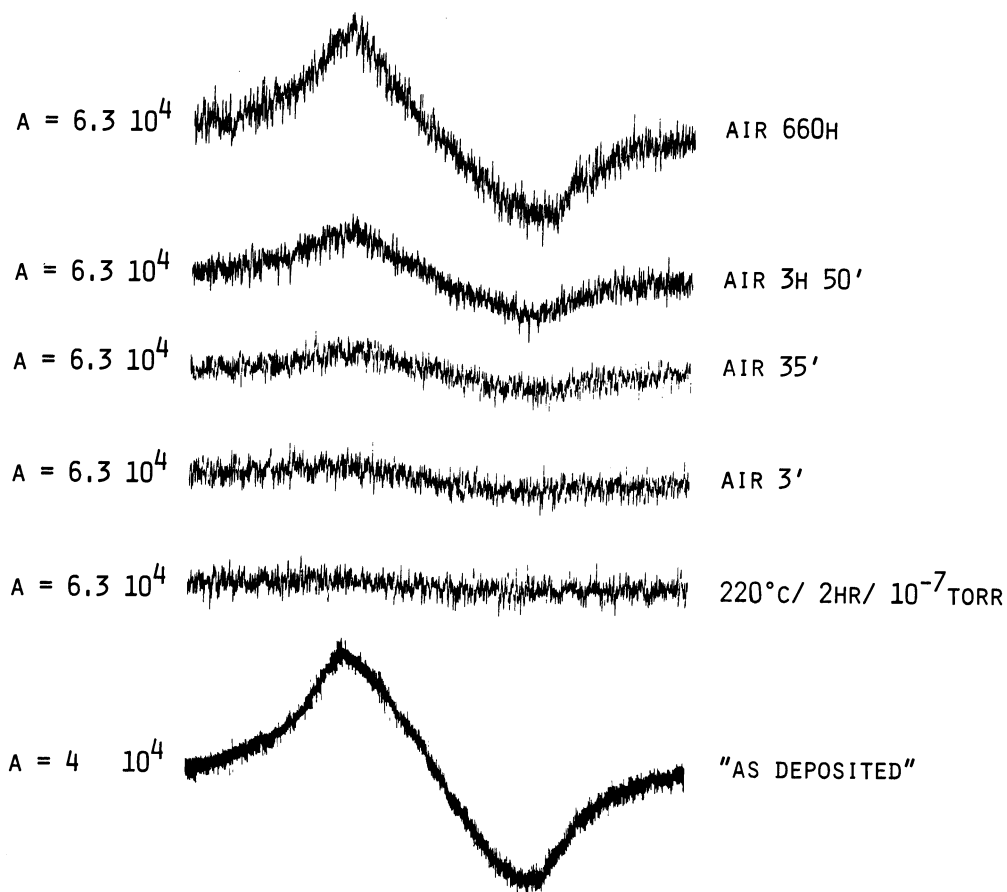


Fig. 12. ESR signal ($g = 2.0055$) of Mo-Si sample which was, after deposition, exposed to air (lower curve), after annealing at 220°C under vacuum (measured under vacuum), and after exposure to air for the indicated period. A is the amplification factor (153).

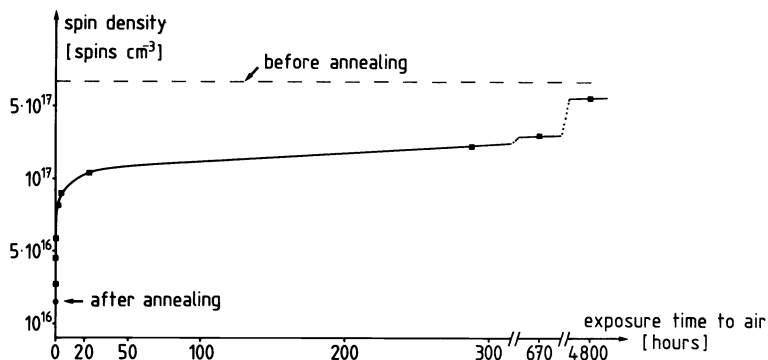


Fig. 13. Electron spin density of Mo-Si as a function of time of exposure to air (144).

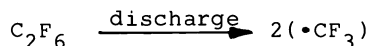
One of the attractive properties of $\mu\text{-Si}$ is the possibility to efficiently change its conductivity by doping and values of $\sigma_{\text{R.T.}}$ of $\sim 10 (\Omega\text{cm})^{-1}$ have been achieved with phosphorus doping (e.g. (76)). Of a particular interest is the result of Spear, et al (76) who have found that $\mu\text{-Si}$ shows normal sign of Hall mobility down to the lower limit of the crystallite size of $\sim 20 \text{ \AA}$ where it reaches zero, and becomes negative for a-Si. Considering their experimental arrangement it is likely that the deposition took place under negative bias of the substrate thus resulting in building up compressive stress in their films. Consequently, the crystallite size of $\sim 20 \text{ \AA}$ is the lower limit of the stability of the crystalline phase in this case (see also (68)).

CONCLUDING REMARKS

The topics covered in the present paper were intentionally rather restricted in order to provide a deeper insight into the control of the structural properties of solids prepared by CVD under plasma conditions. Such a restriction is justified by the importance of the plasma-assisted CVD for industrial applications and the author hopes to have shown that this aspect is now receiving a firm scientific base and a good deal of understanding of the processes has been achieved.

An inherent disadvantage of such an approach is, of course, that many further aspects of preparative solid state chemistry had to be left out. For example, we did not discuss the possibilities of synthesis of novel compounds utilizing the high chemical activity of the low pressure plasma (i.e. the "thermodynamic effect" (11,15,19)) which should allow to prepare solid compounds of unusual stoichiometry. One step towards such syntheses is the preparation of $\text{TiH}_2\text{-}\gamma$ phase under conditions (pressure and temperature) where, at thermodynamic equilibrium, the hydrogen concentration reaches only a few percent (148,149).

Another example is the first synthesis of xenon difluoride by Hoppe, et al (150), and many further successful synthetic applications of plasmas have been found in past years. Worth mentioning is in particular the synthesis of trifluoromethyl organometallic compounds in which case the plasma is used to generate the trifluoromethyl radicals, e.g. by the discharge-induced cleavage of the C-C bond in hexafluoroethane:



The CF_3 -radicals are then allowed to react with metallic halides to yield the desirable organometallic compounds (151-153). Although little understanding of the plasma-chemical processes has been achieved, the variety of interesting new compounds synthesized by this technique is surely encouraging and it shows that it is worthwhile to use the plasma also just as a "black box" in order to open up new areas of preparative chemistry.

Acknowledgement - I should like to express my deep gratitude to my co-workers, in particular to Dr.Z.Iqbal, F.-A.Sarott, Dr.J.J.Wagner, Dr.R.Wild, Dr.A.P.Webb, Dr.R.Brewer, Dr.J.K.Gimzewski and Dr.P.Capezzuto for their enthusiastic work and to Prof.H.R.Oswald for his standing support and encouragement. This work has been supported in part by the Schweizerischer Nationalfonds zur Förderung der wissenschaftlichen Forschung and by the Nationaler Energie-Forschungs-Fonds.

REFERENCES

1. F.Vursel and L.Polak, in: Reactions under Plasma Conditions, ed. M.Venugopalan, Wiley, New York (1971), Vol. 2.
2. B.Eliasson and U.Kogelschatz, Proc. of 4th Int.Symp. on Plasma Chemistry, eds. S.Vepřek and J.Hertz, University of Zürich, Zürich (1979), p. 729.
3. B.Eliasson and U.Kogelschatz, Proc.5th Int.Symp. on Plasma Chemistry, ed. B.Waldie, Heriot-Watt University, Edinburgh (1981), p. 415.
4. J.Salge and P.Braumann, Proc. of 4th Int.Symp. on Plasma Chemistry, eds. S.Vepřek and J.Hertz, University of Zürich, Zürich (1979), p. 735.
5. Proc.Int.Symp. on Ozone and Water, Berlin 1977, O.Hess, Berlin 1978.
6. Ibid, (1981) - to be published.
7. J.R.Hollahan and A.T.Bell (eds.), Techniques and Applications of Plasma Chemistry, Wiley, New York 1974.
8. J.L.Vossen and W.Kern, Thin Film Processes, Academic Press, New York 1978.

9. C.J.Mogab and H.J.Levinstein, J.Vac.Sci.Technol. 17, 721 (1980).
10. Workshop on Plasma Chemistry and Arc Technology, University of Minnesota, Minneapolis (1980).
11. S.Vepřek, Chimia 34, 489 (1980).
12. S.Vepřek and J.Knights, in Ref. (10), p. 57.
13. J.R.Hollahan and R.S.Rosler, in Ref. (8), p. 335.
14. H.Drost, Plasmachemie, Akademie-Verlag, Berlin (1978).
15. S.Vepřek, J.Chem.Phys. 57, 952 (1972).
16. S.Vepřek and W.Peier, Chem.Phys. 2, 478 (1973).
17. S.Vepřek, J.Crystal Growth 17, 101 (1972).
18. S.Vepřek, Z.f.phys.Chem., N.F. 86, 95 (1973).
19. S.Vepřek, in: Topics in Current Chemistry, Vol. 56, Springer-Verlag, Berlin (1975).
20. S.Vepřek, Pure Appl.Chem. 48, 163 (1976).
21. D.A.Anderson, Phil.Mag. 35, 17 (1977).
22. C.T.Wendel and M.H.Wiley, J.Polymer Sci. 10, 1069 (1972).
23. D.S.Whitmell and R.Williamson, Thin Solid Films 35, 255 (1976).
24. L.Holland and S.M.Ojha, Thin Solid Films 38, L17 (1976); 40, L31 (1977); 48, L21 (1978).
25. R.J.Gambino and J.A.Thompson, Solid St.Comm. 34, 15 (1980).
26. D.I.Jones and A.D.Stewart, Proc. 9th Int.Conf. on Amorph. and Liquid Semiconductors, Grenoble 1981 (to be publ. in J.Physique).
27. S.A.Solin, N.Wada and J.Wong, Inst.Phys.Conf.Ser. No. 43, 721 (1979).
28. N.Wada, P.J.Gaczi and S.A.Solin, J.Non-Cryst.Solids 35 & 36, 543 (1980).
29. H.Krebs, Grundzüge der anorganischen Kristallchemie, F.Enke-Verlag, Stuttgart (1968).
30. H.G.von Schnering, in: Homoatomic Rings, Chains and Macromolecules of Main-Group Elements, ed. A.L.Rheingold, Elsevier Amsterdam (1977).
31. H.U.Beyeler and S.Vepřek, Phil.Mag. B41, 327 (1980).
32. S.Vepřek and H.R.Oswald, Z.anorg.allg.Chem. 412, 190 (1975).
33. S.Vepřek, Habilitationsschrift, University of Zürich (1977).
34. R.Wild, Ph.D.Thesis, University of Zürich (1979).
35. J.Brunner, M.Thüler, S.Vepřek and R.Wild, J.Phys.Chem.Solids 40, 967 (1979).
36. W.E.Spear, P.G.Le Comber, S.Vepřek and R.Wild, Phil.Mag. B38, 349 (1978).
37. E.V.Borisov and E.E.Nifantev, Usp.Khim. 46, 1604 (1977).
38. S.Vepřek, Z.Iqbal, J.Brunner and M.Schärli, Phil.Mag. B43, 527 (1981).
39. J.Ogier, Ann.Chim. 20, 32 (1880).
40. R.Schwarz and F.Heinrich, Z.anorg.allg.Chem. 221, 277 (1935).
41. E.J.Spanier and A.G.McDiarmid, Inorg.Chem. 2, 215 (1963).
42. J.E.Drake and W.I.Jolly, Chem. and Ind. 1470 (1962).
43. S.D.Gokdale and W.I.Jolly, Inorg.Chem. 3, 946, 1141 (1964); 4, 596 (1965).
44. S.Vepřek and V.Mareček, Solid State Electronics 11, 683 (1968).
45. P.C.Chittick, J.H.Alexander and H.F.Sterling, J.Electrochem.Soc. 116, 77 (1969).
46. N.F.Mott and E.A.Davis, Electronic Processes in Non-Crystalline Solids, 1st Ed., Clarendon Press, Oxford (1971); 2nd Ed. 1979.
47. W.E.Spear and P.G.Le Comber, J.Non-Cryst.Solids 8-10, 727 (1972).
48. W.E.Spear, in: Proc. 5th Int.Conf. on Amorph. and Liquid Semiconductors, eds. J.Stuke and W.Brenig, Taylor and Francis, London (1974), p. 1.
49. W.E.Spear and P.G.Le Comber, Solid St.Comm. 17, 1193 (1975) and Phil.Mag. B33, 935 (1976).
50. W.E.Spear, Adv.Phys. 26, 811 (1977).
51. D.E.Carlson and C.R.Wronski, Appl.Phys.Lett. 28, 671 (1976).
52. D.E.Carlson: U.S.Patent No. 4, 064, 521 (1977).
53. M.H.Brodsky, ed.: Amorphous Semiconductors (Topics in Appl.Phys. Vol. 36) Springer-Verlag, Berlin (1979).
54. D.E.Carlson, in Ref. (53).
55. D.E.Carlson, Solar Energy Materials 3, 503 (1980).
56. Proc. 9th Int.Conf. on Amorph. and Liquid Semiconductors, Grenoble July 1981, to be publ. in J.Physique.
57. Y.Hamakawa, in Ref. (56).
58. W.E.Spear, *ibid.*
59. Y.Kuwano, *ibid.*
60. Y.Tawada, M.Kondo, H.Okamoto and Y.Hamakawa, Proc. 15th IEEE Photovoltaic Specialists Conf. Florida (1981).
61. D.E.Carlson (1981) private communication.
62. P.G.Le Comber, A.J.Snell, K.D.Mackenzie and W.E.Spear, in Ref. (56).
63. D.J.Di Maria, *ibid.*
64. I.Shimizu, S.Oda, K.Sato, H.Tomita and E.Inoue, *ibid.*
65. Z.Iqbal, A.P.Webb and S.Vepřek, Appl.Phys.Lett. 36, 163 (1980).
66. S.Vepřek, Z.Iqbal, H.R.Oswald and A.P.Webb, J.Phys.C: Solid State Phys. 14, 295 (1981).
67. Z.Iqbal, S.Vepřek, A.P.Webb and P.Capezzuto, Solid St.Comm. 36, 993 (1981).

68. S.Vepřek, Z.Iqbal and F.A.Sarott, Phil.Mag.B (1981) in press.
69. S.Vepřek, Z.Iqbal, H.R.Oswald, F.A.Sarott, J.J.Wagner and A.P.Webb, Solid State Commun. 39, 509 (1981).
70. S.Vepřek, Z.Iqbal, H.R.Oswald, F.A.Sarott and J.J.Wagner, in Ref. (56).
71. Z.Iqbal and S.Vepřek, J.Phys.C: Solid State Phys. (1981) in press.
72. Z.Iqbal, P.Capezzuto, M.Braun, H.R.Oswald, S.Vepřek, G.Brunno, F.Cramarossa, H.Stüssi, J.Brunner and M.Schärli, Thin Solid Films (1981) in press.
73. S.Usui and M.Kikuchi, J.Non-Cryst.Solids 34, 1 (1979).
74. F.Morin and M.Morel, Appl.Phys.Lett. 35, 686 (1979).
75. A.Matsuda, S.Yamasaki, K.Nakagava, H.Okushi, K.Tanaka, S.Izima, M.Matsumura and H.Yamamoto, Jap.J.Appl.Phys. 19, L305 (1980).
76. W.E.Spear, G.Willeke, P.G.Le Comber and A.G.Fitzgerald, in Ref. (56).
77. A.P.Webb and S.Vepřek, Chem.Phys.Lett. 62, 173 (1978).
78. S.Vepřek and A.P.Webb, Proc. 4th Int.Symp. on Plasma Chemistry, Univ. of Zürich (1979), eds. S.Vepřek and J.Hertz, p. 79.
79. D.R.Stuhl and H.Prophet, JANAF Thermochemical Tables, 2nd Ed., Nat.Bureau of Standards publication NSRDS-NBS 37, Washington, D.C. (1971).
80. D.R.Olander (1980) private communication.
81. P.Neudorfi, A.Jodhan and O.P.Strausz, J.Phys.Chem. 84, 338 (1980)
82. D.Berthelot and H.Gaudechon, Compt.rend. 156, 1243 (1913).
83. I.Dubois, Canad.J.Phys. 46, 2485 (1968).
84. H.J.Emeléus and K.Stewart, Trans.Farad.Soc. 32, 1577 (1936).
85. D.White and E.G.Rochow, J.Am.Chem.Soc. 76, 3897 (1954).
86. H.Niki and G.J.Mains, J.Phys.Chem. 68, 304 (1964).
87. M.A.Nay, G.N.C.Woodall, O.P.Strausz and H.E.Gunning, J.Am.Chem.Soc. 87, 179 (1965).
88. T.F.Deutsch, J.Chem.Phys. 70, 1187 (1979).
89. S.Vepřek, J.Chem.Phys. 57, 952 (1972).
90. S.Vepřek, in: Topics in Current Chemistry, Vol. 56, Springer-Verlag, Berlin 1975.
91. H.F.Winters, in: Plasma Chemistry III, eds. S.Vepřek and M.Venugopalan, Springer-Verlag, Berlin 1980.
92. P.Glansdorff and I.Prigogine, Thermodynamic Theory of Structure, Stability and Fluctuations, J.Wiley, London 1971.
93. S.Vepřek and W.Peier, Chem.Phys. 2, 478 (1973).
94. N.L.Arthur and T.N.Bell, Rev. of Chemical Intermediates 2, 37 (1978).
95. J.H.Lee, J.V.Michael, W.A.Payne, D.A.Whytock and L.J.Stief, J.Chem.Phys. 65, 3280 (1976).
96. M.Balooch and D.R.Olander, J.Chem.Phys. 63, 4772 (1975).
97. M.Cardona and L.Ley, eds., Photoemission in Solids (Topics in Appl.Phys. Vol. 26 and 27), Springer-Verlag, Berlin 1978.
98. T.Sakurai and H.D.Hagstrum, Phys.Rev.B 12, 5349 (1975); 14, 1593 (1976).
99. T.Sakurai and H.D.Hagstrum, J.Vac.Sci.Technol. 13, 807 (1976).
100. K.C.Pandey, T.Sakurai and H.D.Hagstrum, Phys.Rev.Lett. 35, 1728 (1975).
101. H.Wagner, R.Butz, U.Backes and D.Bruchmann, Solid St.Commun. (1981) in press, and 41st Annual Conf. on Phys.Electron., Montana State Univ., Bozeman, Montana (1981).
102. R.Butz, R.Memeo, H.Wagner, U.Backes and D.Bruchmann, ECOSS 4, Münster (F.R.G.) (1981).
103. D.C.Allan and J.D.Joannopoulos, Phys.Rev.Lett. 44, 43 (1980).
104. F.-A.Sarott, Diplomarbeit, University of Zürich (1981).
105. B.Drevillon, J.Huc, A.Lloret, J.Perrin, G.de Rosny and J.P.M.Schmitt, Appl.Phys.Lett. 37, 646 (1980).
106. G.Turban, Y.Catherine and B.Grolleau, Thin Solid Films, 67, 309 (1980); 77, 287 (1981).
107. G.Turban, Y.Catherine and B.Grolleau, Plasma Chem. and Plasma Processing (to be publ.).
108. I.Haller, Appl.Phys.Lett. 37, 282 (1980).
109. D.A.Baldvin, P.T.Murray and J.W.Rabalais, Chem.Phys.Lett. 77, 403 (1981).
110. C.I.H.Ashby and R.R.Rye, J.Nucl.Materials 92, 141 (1980).
111. J.P.Hirth and G.M.Pound, Condensation and Evaporation, Pergamon Press, London (1963).
112. R.Grigorovici and R.Manaila, J.Non-Cryst.Solids 1, 371 (1969).
113. R.Grigorovici, in: Amorphous and Liquid Semiconductors, ed. J.Tauc, Plenum Press, London 1974.
114. R.Grigorovici, in: Electronic and Structural Properties of Amorphous Semiconductors, eds. P.G.Le Comber and J.Mort, Academic Press, London 1973.
115. J.G.Allpress and J.V.Sanders, Aust.J.Phys. 23, 23 (1970).
116. M.P.Hoare and P.Paul, Adv. in Phys. 24, 645 (1975).
117. Y.Takasu and A.M.Bradshaw, in: Chem.Phys. of Solids and their Surfaces, Vol. 7, Chem.Soc., London (1978).

118. R. Mosseri and J.P. Gaspard: in Ref. (56).
119. P. Gaskell, J. Phys. C: Solid St. Phys. 17, 4337 (1979).
120. H. Schäfer, Chemical Transport Reactions, Verlag Chemie, Weinheim (1962); Academic Press, New York (1964).
121. J.J. Wagner and S. Vepřek, 5th Int. Symp. on Plasma Chemistry, Edinburgh 1981, and to be published.
122. W.G. Townsend and M.E. Uddin, Solid St. Electronics 16, 39 (1973).
123. G.A. Melin and P.J. Madix, Trans. Farad. Soc. 67, 198; 2711 (1971).
124. R. Dandoloff, Ph. Dr. Thesis, Max-Planck-Institut für Festkörperforschung, Stuttgart (F.R.G.) 1981.
125. R. Dandoloff, G. Döhler and H. Bilz, J. Non-Cryst. Solids 35 & 36, 537 (1980).
126. G. Döhler, R. Dandoloff and H. Bilz, ibid., 42, 87 (1980).
127. G. Nolet, J. Electrochem. Soc. 122, 1030 (1975).
128. Tung-Yang Yu, T.M.H. Cheng, V. Kempter and F.W. Lampe, J. Phys. Chem. 76, 3321 (1972).
129. J. Perrin and E. Delafosse, J. Phys. D: Appl. Phys. 13, 759 (1980).
130. M. Capitelli and E. Molinari, in: Plasma Chemistry II, eds. S. Vepřek and M. Venugopalan, Springer-Verlag, Berlin 1980.
131. N.H. Tolk, J.C. Tully, W. Heiland and C.W. White, eds., Inelastic Ion-Surface Collisions, Academic Press, New York 1977.
132. P.G. Le Comber, A. Madan and W.E. Spear, J. Non-Cryst. Solids 11, 219 (1972).
133. D.I. Jones, R.A. Gibson, P.G. Le Comber and W.E. Spear, Solar En. Materials 2, 93 (1979).
134. J.C. Knights, G. Lucovsky and R.J. Nemanich, J. Non-Cryst. Materials 32, 393 (1979).
135. J.C. Knights and R.A. Lujan, Appl. Phys. Lett. 35, 244 (1979).
136. J.C. Knights, J. Non-Cryst. Materials 35 & 36, 159 (1980).
137. Proc. 8th Int. Conf. on Amorph. and Liquid Semicond., W. Paul and M. Kastner, eds., North-Holland, Amsterdam 1980 (J. Non-Cryst. Mater. 35 & 36 (1980)).
138. H. Fritzsche, Solar En. Materials 3, 447 (1980).
139. D.R. Uhlmann, Inorganic Amorphous Solids and Glass-Ceramic Materials, in: N.B. Hannay, Treatise on Solid State Chemistry, Vol. 3, Chapt. 5, Plenum Press, New York 1976.
140. W. Vogel: Glaschemie (VEB Deutscher Verlag für Grundstoffindustrie, Leipzig 1979).
141. H. Richter and L. Ley, J. Appl. Phys. (submitted).
142. Z. Iqbal and S. Vepřek (to be published).
143. R. Tsu, M. Izu, S.R. Ovshinsky and F.H. Pollak, Solid St. Commun. 36, 817 (1980).
144. S. Vepřek, Z. Iqbal, O. Kühne and P. Capezuto (submitted).
145. T.I. Kamins, J. Appl. Phys. 42, 4357 (1971).
146. J.Y.W. Seto, J. Appl. Phys. 46, 5247 (1975).
147. G. Baccarani, B. Ricco and G. Spadini, J. Appl. Phys. 49, 5565 (1978).
148. J.K. Gimzewski, R.J. Brewer, S. Vepřek and H. Stüssi, Proc. 5th Int. Symp. on Plasma Chem., ed. B. Waldie, Heriot-Watt University, Edinburgh (1981).
149. R.J. Brewer, J.K. Gimzewski, S. Vepřek and H. Stüssi, J. Nucl. Materials (1981) (in press).
150. R. Hoppe, H. Mattauch, K.M. Rödder and W. Dähne, Z. anorg. allg. Chem. 324, 214 (1963).
151. R.J. Lagow and J.A. Morrison, Adv. in Inorg. Chem. and Radiochem. 23, 177 (1980).
152. L.J. Turbini, R.E. Aikman and R.J. Lagow, J. Amer. Chem. Soc. 101, 5833 (1979).
153. R.J. Lagow, L.L. Gerchman, R.A. Jacob and J.A. Morrison, J. Amer. Chem. Soc. 97, 518 (1975).